Supporting Information for:

Modular Metallotecton for Engineering Porous Supramolecular Frameworks: Supernumerary Role of Ancillary Ion

Deepak Gupta, Géraldine Chanteux, Gulshan Kumar[⊥], Koen Robeyns and Alexandru Vlad*.

Institute of Condensed Matter and Nanosciences, Molecular Chemistry, Materials and Catalysis, Université catholique de Louvain, Louvain-la-Neuve B-1348, Belgium

[⊥]Present Address: Fraunhofer Institute of Interfacial Engineering and Biotechnology IGB, Bio-, Electro-, and Chemocatalysis BioCat, Straubing Branch, Schulgasse 11a, 94315, Straubing, Germany

Email: alexandru.vlad@uclouvain.be

Table of Content

Material and Methods

All following chemicals were purchased and used as received. $RuCl_3.xH_2O$ (40-43% Ru) was purchased from Strem Chemicals. 1,10-phenanthroline (98%), ammonium hexafuorophosphate (99%) and nitric acid (65%) were purchased from Fluorochem. Absolute ethanol and chloroform stabilized with ~0.6% ethanol were purchased from VWR. Potassium bromide (99+%) was purchased from Alfa Aesar. Methanol (99.8%) extra dry over molecular sieve, N,N-dimethylformamide (99.8%) extra dry over molecular sieve and tetrabutylammonium bromide (99+%) were purchased from Thermoscientific. Dithiooxamide (97%), lithium methoxide (98%) and anhydrous dimethyl sulfoxide (>99.9%) were purchased from Sigma Aldrich. The synthesis of 1,10-phenanthroline-5,6-dione, $Ru(DMSO)_4Cl_2$ and [Ru(1,10-phenanthroline-5,6-dione)$_3$].2Cl were performed using reported procedures.[1-5]

FTIR spectroscopy was carried out on a Bruker Alpha P spectrometer with a single reflection ATR module. ^{1}H NMR and ^{13}C NMR spectra were recorded on a Bruker Avance II 300 spectrometer (at 300 and 75 MHz, respectively) at 298 K. Chemical shifts are given in ppm relative to TMS. Single X-ray diffraction data were recorded on an MAR345 image plate, using Mo Kα radiation (λ= 0.71073 Å) generated by an Incoatec microfocus source (Montel optics). Data integration and reduction was performed by CrysAlis^{PRO} Software System1, Version 1.171.37.35. Rigaku Oxford Diffraction and the implemented absorption correction was applied.[6,7] The structure was solved by SHELXT and refined by least-squares against F^2 by shelxt2018/3.[8,9] All non-hydrogen atoms were refined anisotropically and hydrogens were placed at calculated positions and refined in riding mode with temperature factors set at 1.2 Ueq of the parent atoms (1.5 for methyl groups). Void cavities were treated by the Squeeze algorithm as implemented in PLATON (Spek). **1.Cl** was refined as twinned by inversion, with a refined twin fraction of 50%. For **1.Br** and **1.Li** a resolution cut-off to 0.9Å and 1 Å, respectively, was imposed during integration. In **1.Br** the bromide anion is found disordered over two sites and competes with a water molecule resulting in two mixed sites Br/H_2O in a 75/25 and 25/75 ratio respectively. **1.Li** was also found to be twinned and was refined against HKLF5 formatted reflection data. For both **1.Br** and **1.Li**, due to the restricted resolution of the data, overall isotropic and rigid bond restraints were applied.

Powder X-ray diffraction data were recorded were recorded using a STOE Stadi P diffractometer equipped with a Mo anticathode (Kα radiation, 0.71073 Å; 50 kV, 40 mA) in the range of 2θ = 1-50° , with a step size of 1° and 50 s acquisition time per step.

Thermogravimetric analyses (TGA) were performed on a TGA/DSC 3+ from Mettler

Toledo equipped with a LF1100 oven (1100°C) and a GC 401 gas controller (air and N_2). The samples (2-4 mg) were weighed and placed into 70 µL alumina containers. They were heated at 10 °C/min from 25°C to 850°C under nitrogen flow (100 mL/min).

Synthetic procedures

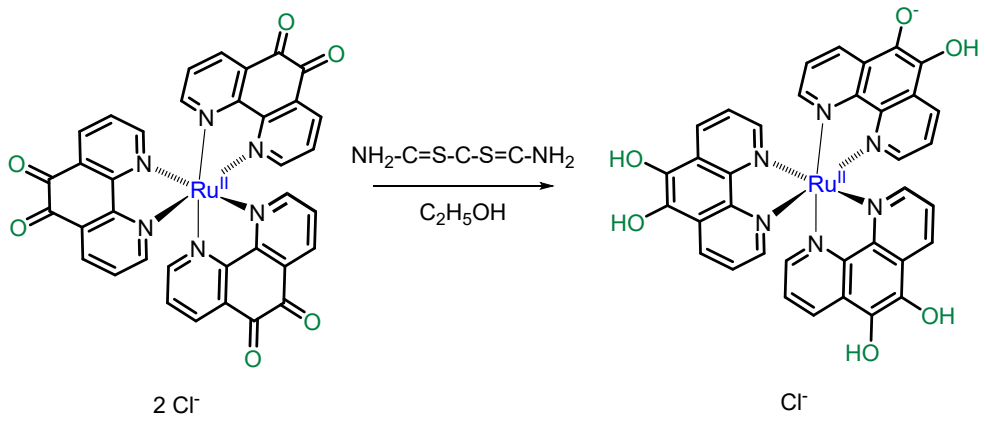

Scheme S1: Synthetic route to **1.Cl**.

[Ru(1,10-phenanthroline-5,6-dione)$_3$].2Cl (0.3 mmol) and dithiooxamide (2.4 mmol) were suspended in ethanol (20 mL) in a 50 mL flask. The reaction mixture was bubbled with argon for 15 minutes and allowed to reflux for 24 hrs in dark under argon. The appearance of bright orange powder on the walls was indicative of product formation. After cooling the reaction to RT, the orange powder was filtered, and washed with fresh diethyl ether (10 mL) under argon. The product was dried in vacuo at 70°C overnight, under dark. Yield (89%).

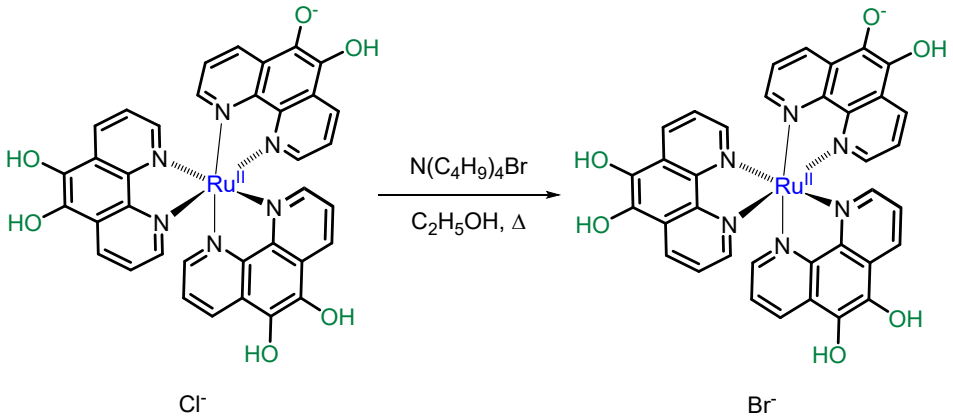

Scheme S2: Synthetic route to **1.Br**.

Under argon atmosphere, [Ru(1,10-phenanthroline-5,6-diol)$_3$].2Cl (0.6 mmol) was dissolved in 50 ml ethanol in a 100 ml flask followed by the addition of ethanolic solution of tetrabutylammonium bromide (0.7 mmol). The reaction mixture was bubbled with argon for 15 minutes and allowed to reflux overnight. The dark brown powder was washed three times with dry ether, transferred in the glove box and dried at 100°C for 12 hours. Yield (84%).

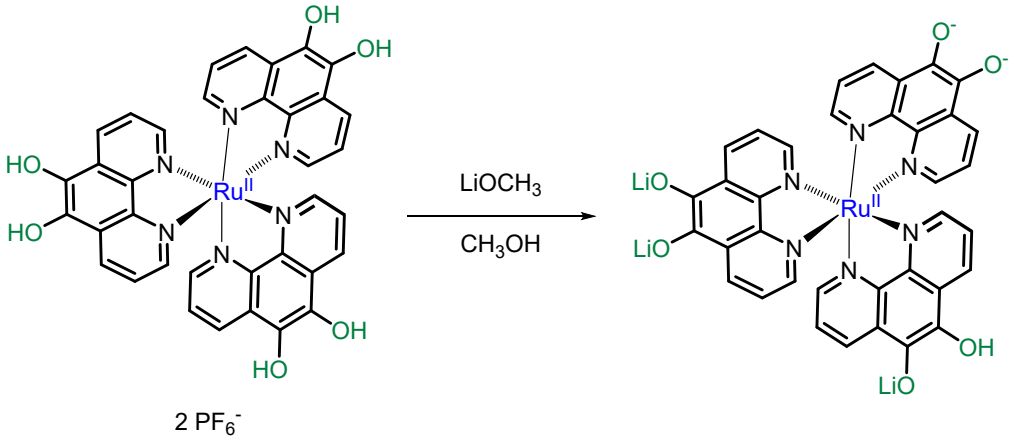

Scheme S3: Synthetic route to **1.Li**.

Lithium methoxide (1.6 mmol) was dissolved in 20 mL of dry methanol under argon. To this, [Ru(5,6-dihydroxy-1,10-phenanthroline)$_3$].2PF$_6$ (0.2 mmol) was added in portions with stirring to obtain a dark brown clear solution at RT. This was left for stirring for 2 days under dark. The dark brown product was precipitated by adding the reaction mixture to diethyl ether (50 mL). The product was centrifuged, washed with diethyl ether and dried in vacuo at 70°C overnight under dark. Yield (93%).

Note: [Ru(5,6-dihydroxy-1,10-phenanthroline)$_3$].2PF$_6$ can be directly obtained from [Ru(5,6-dihydroxy-1,10-phenanthroline)$_3$].2Cl by anion exchange method.

Crystallization procedures

Single crystals of **1.Cl** and **1.Br** were grown by dissolving the complexes in methanol at RT under argon atmosphere. The orange saturated solution was passed through a 5 μm filter to remove any aggregates. A 1 mL aliquot of the solution was kept in a transparent vial (3 mL) which was placed in another vial (30 mL) containing 5 mL of diethyl ether to allow slow diffusion of ether into the methanolic solution. The vial was tightly capped and left undisturbed for one week in the dark. Orange colored, needle-shaped crystals, suitable for single crystal analysis, were observed on the walls.

Single crystals of **1.Li** were obtained by dissolving Li_4[Ru(1,10-phenanthroline-5,6-dioxide)] in anhydrous methanol under inert atmosphere. The brown saturated solution was passed through a 5 μm filter to remove any aggregates. A 1 mL aliquot of this solution was layered over 1 mL of DMF in a 3 mL vial which was tightly capped and left undisturbed for three weeks. The layers were found to be mixed completely to give a clear brown solution. The vial cap was unscrewed slightly and allowed the solvent to evaporate slowly. At an optimum concentration, shiny block like crystals started to appear in the solution. A small amount of mother liquid with single crystals was pipetted in paratone® oil to avoid decomposition, prior to flash cooling in a 120K or 150K N_2 stream.

Exchange and inclusion studies

The weighed amount of compounds **1.Cl** and **1.Br** were heated up to 80 ^oC under vacuum for 6 hrs to remove residual solvent molecules. Subsequently, the desolvated compounds were allowed to equilibrate in a sealed environment of D_2O and I_2 vapors separately.

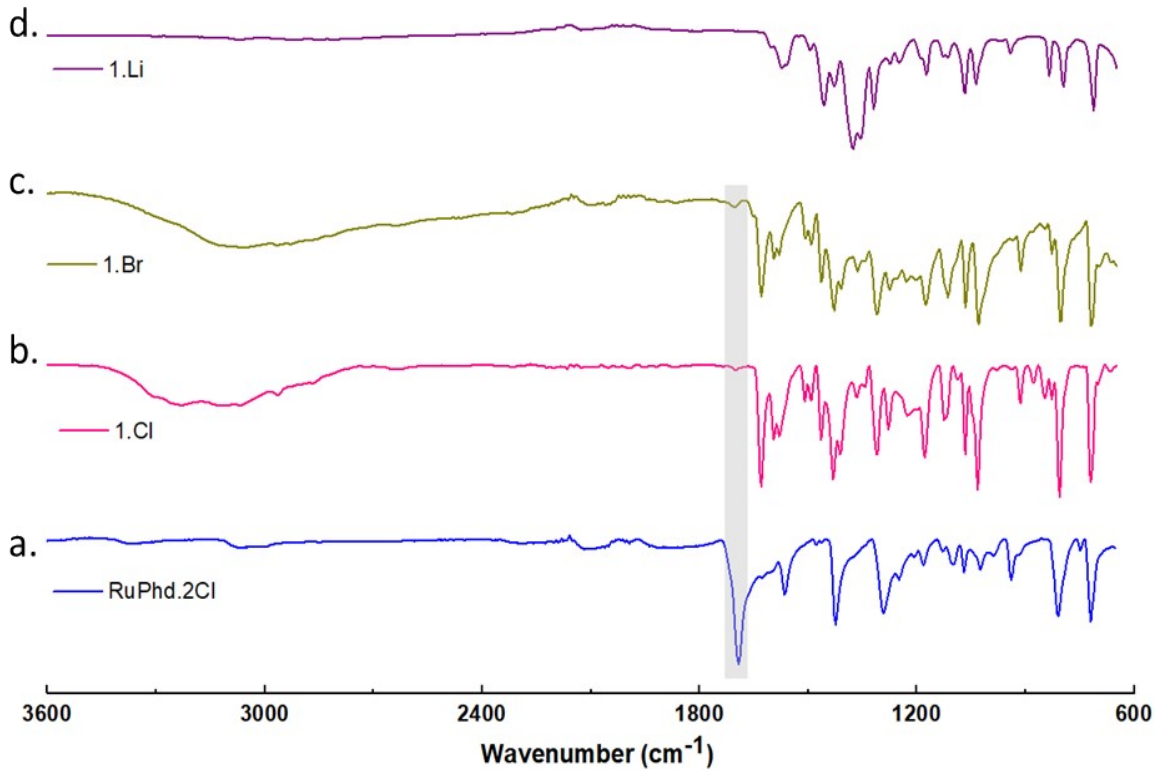

Figure S1: FTIR spectra of [Ru(1,10-phenanthroline-5,6-dione)$_3$].2Cl (a), **1.Cl** (b) **1.Br** (c) and **1.Li** (d). The band corresponding to the C=O group is highlighted in grey.

The FTIR spectrum of the three supramolecular frameworks (**1.Cl**, **1.Br** and **1.Li**) as well as the starting material [Ru(1,10-phenanthroline-5,6-dione)$_3$].2Cl were recorded in solid state; wherein the disappearance of the intense carbonyl band at 1694 cm^{-1} and appearance of a broad band in the region 3000-3300 cm^{-1} (in **1.Cl** and **1.Br**) confirmed the product formation. No other significant change was observed.

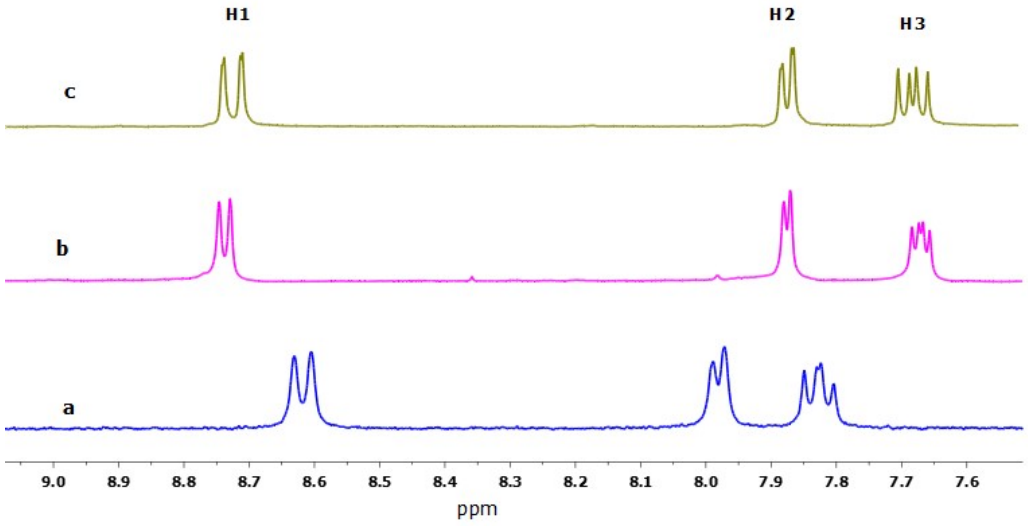

Figure S2: Selected region ^{1}H NMR of the complexes (a) [Ru(1,10-phenanthroline-5,6-dione)$_3$].2Cl (a), **1.Cl** (b) and **1.Br** (c) in DMSO-d_6.

The ^{1}H NMR spectra (400 MHz) of the starting complex [Ru(1,10-phenanthroline-5,6-dione)$_3$].2Cl and **1.Cl** and **1.Br** were recorded in DMSO-d_6. The spectra established the product formation by increase in separation of the signals attributed to the aromatic protons. The shift in peak position is because of alteration in the electronic arrangement in the ligand framework upon reduction of the carbonyl groups to hydroxyl groups.

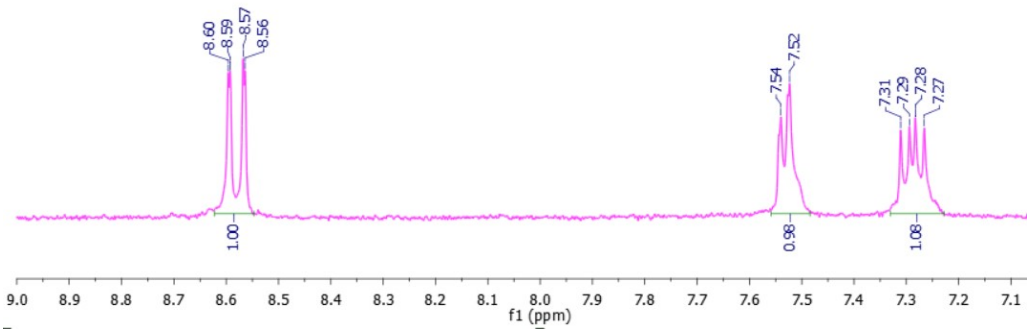

Figure S3: Selected region ^{1}H NMR (400 MHz) spectrum of **1.Li** in CD_3OD.

The ^{1}H NMR spectra (400 MHz) of **1.Li** was performed in CD_3OD which displayed three distinct signals for the three aromatic protons on the phenanthroline ligand confirming the product formation as well as high purity of the final lithiated product. The sample was prepared under inert atmosphere and protected from stray light to avoid degradation of the product.

Table S1: Crystal data and structure refinement parameters for **1.Cl**, **1.Br** and **1.Li**.

Identification code	**1.Cl**	**1.Br**	**1.Li**
Empirical formula	C36 H23 Cl N6 O12 Ru	C36 H23 Br N6 O8 Ru	C45 H39 Li N9 O9 Ru
Formula weight	868.12	848.58	957.86
Temperature	120(2) K	150(2) K	150(2) K
Wavelength	0.71073 Å	0.71073 Å	0.71073 Å
Crystal system	Trigonal	Monoclinic	Monoclinic
Space group	*P*31*c*	$P2_1/n$	$P2_1/n$
Unit cell dimensions	*a* = 16.0468(4) Å	a = 9.5706(5) Å	a = 13.2103(17) Å
	b = *a*	b = 27.2115(13) Å	b = 12.687(2) Å
	c = 9.8253(3) Å	c = 16.1676(10) Å	c = 25.365(4) Å
		β= 90.702(5)°.	β= 99.389(14)°.
Volume	2191.05(13) $Å^3$	4210.2(4) $Å^3$	4194.3(11) $Å^3$
Z	2	4	4
Density (calculated)	1.316 mg/m^3	1.339 mg/m^3	1.517 mg/m^3
Absorption coefficient	0.480 mm^{-1}	1.372 mm^{-1}	0.444 mm^{-1}
F(000)	876	1696	1964
Crystal size	0.25 x 0.04 x 0.03 mm^3	0.50 x 0.05 x 0.04 mm^3	0.06 x 0.04 x 0.01 mm^3
θ range for data collection	3.591 to 25.240°	2.256 to 23.256°	2.922 to 20.965°
Reflections collected	11889	20916	4357
Independent reflections	2637 [$R_{(int)}$ = 0.0469]	5860 [$R_{(int)}$ = 0.1129]	4357 [$R_{(int)}$ = 0]*
Completeness 2θ = 25.240°	99.5 %	97.0 %	97.0 %
Absorption correction	Semi-empirical from equivalents	Semi-empirical from equivalents	Semi-empirical from equivalents
Max. and min. transmission	1.00000 and 0.71516	1.00000 and 0.84305	1.00000 and 0.74138
Refinement method	Full-matrix least-squares on F^2	Full-matrix least-squares on F^2	Full-matrix least-squares on F^2
Data / restraints / parameters	2637 / 1 / 170	5860 / 438 / 476	4357 / 488 / 544
Goodness-of-fit on F^2	1.087	1.023	1.068
Final R indices [I>2sigma(I)]	R_1 = 0.0613, wR_2 = 0.1505	R_1 = 0.0717, wR_2 = 0.1709	R_1 = 0.1210, wR_2 = 0.2421
R indices (all data)	R_1 = 0.0635, wR_2 = 0.1520	R_1 = 0.1254, wR_2 = 0.1990	R_1 = 0.2020, wR_2 = 0.2834
Δρ (max, min)	1.619 and -0.462 e.$Å^{-3}$	0.975 and -0.499 e.$Å^{-3}$	1.267 and -0.897 e.$Å^{-3}$
CCDC No.	2143383	2143384	2143385

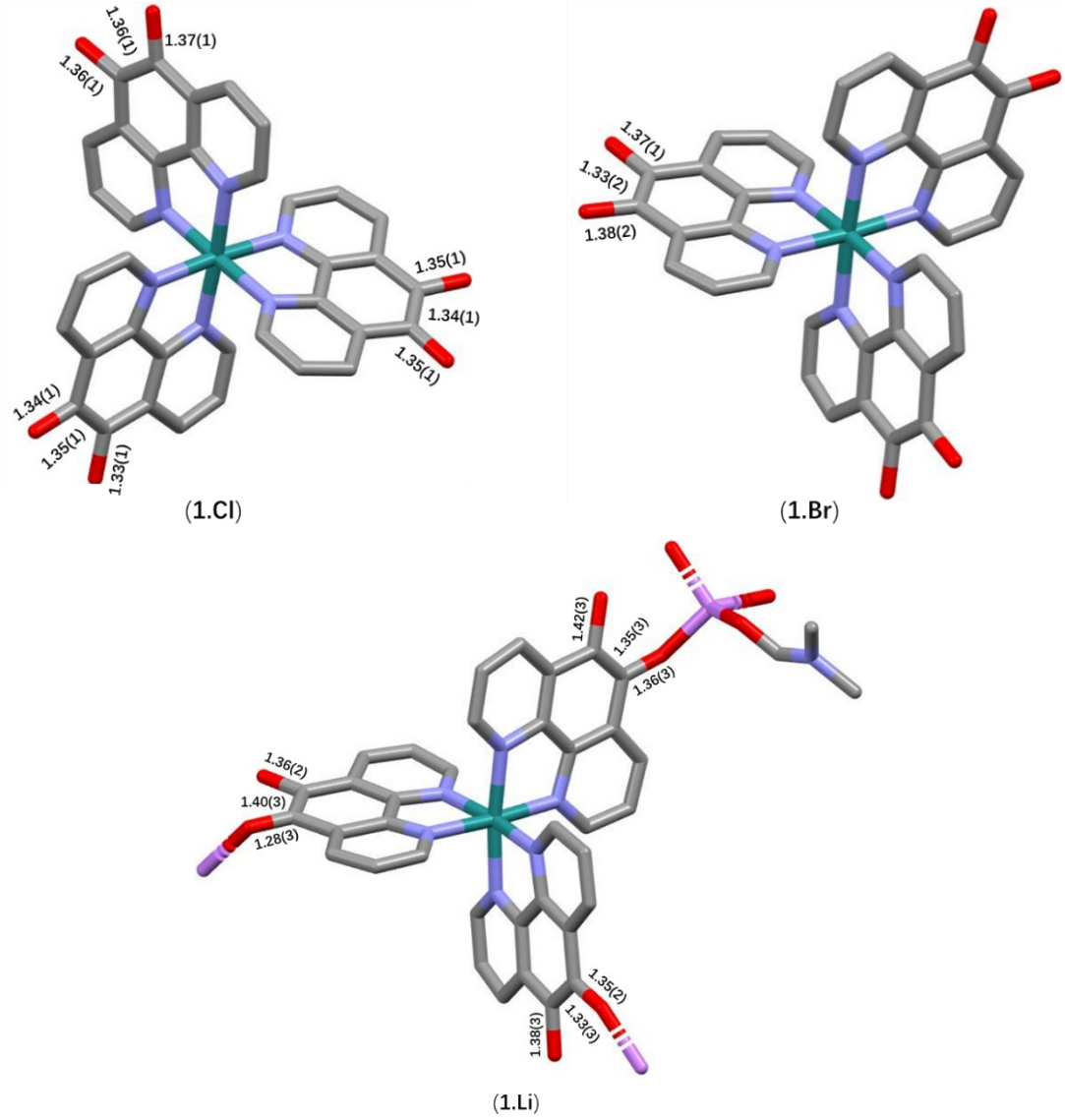

Figure S4: The various bond length parameters in one unit of **1.Cl**, **1.Br** and **1.Li**.

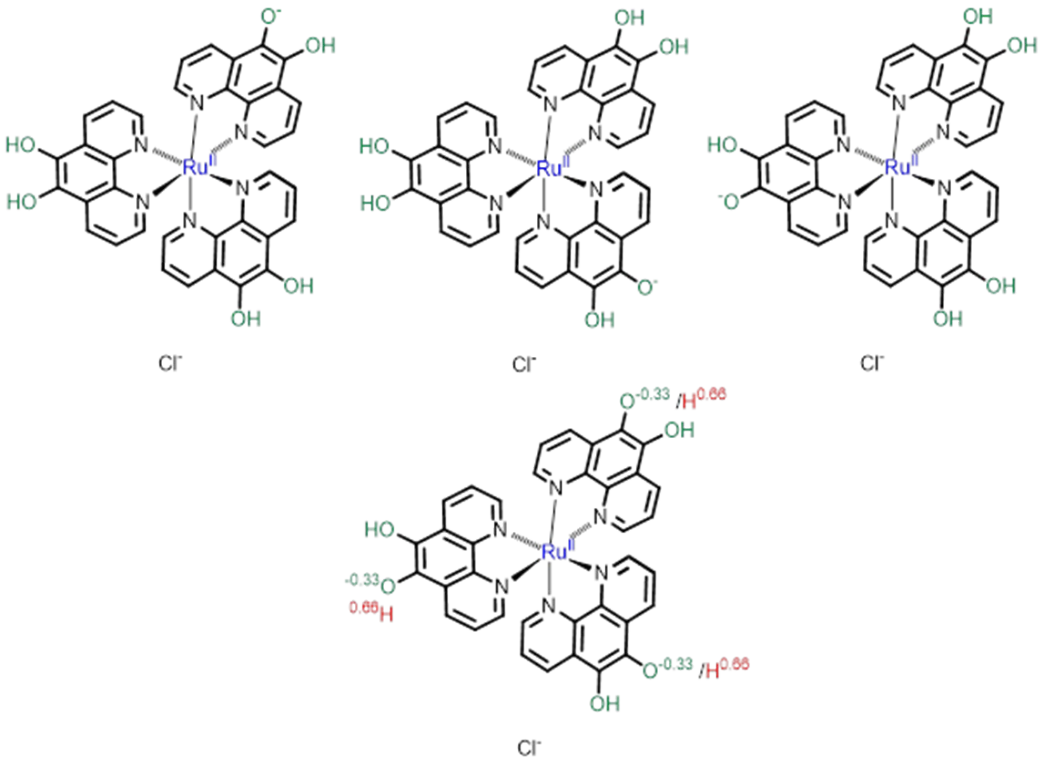

Figure S5: (top) The 3 possible conformations for the Ru complex in **1.Cl**. (Bottom) the occupancy of the hydrogens in the crystal.

In **1.Cl** both the Cl^- anion as well as the Ru complex cation are found on a 3-fold axis. This implies that the overall positive charge of the Ru(II)-complex is achieved by one negative charge on one of the coordinating ligands which can be represented by the chemical formula RuL_2L^-. Crystallographically, all the three ligands are equivalent and the negative charge is assumed to be distributed over the whole Ru-complex unit. This can be explained by constraining the occupancy of the hydrogen atom which is not involved in a hydrogen bond with Cl^- at 0.66, or one O^- out of the six OH groups.

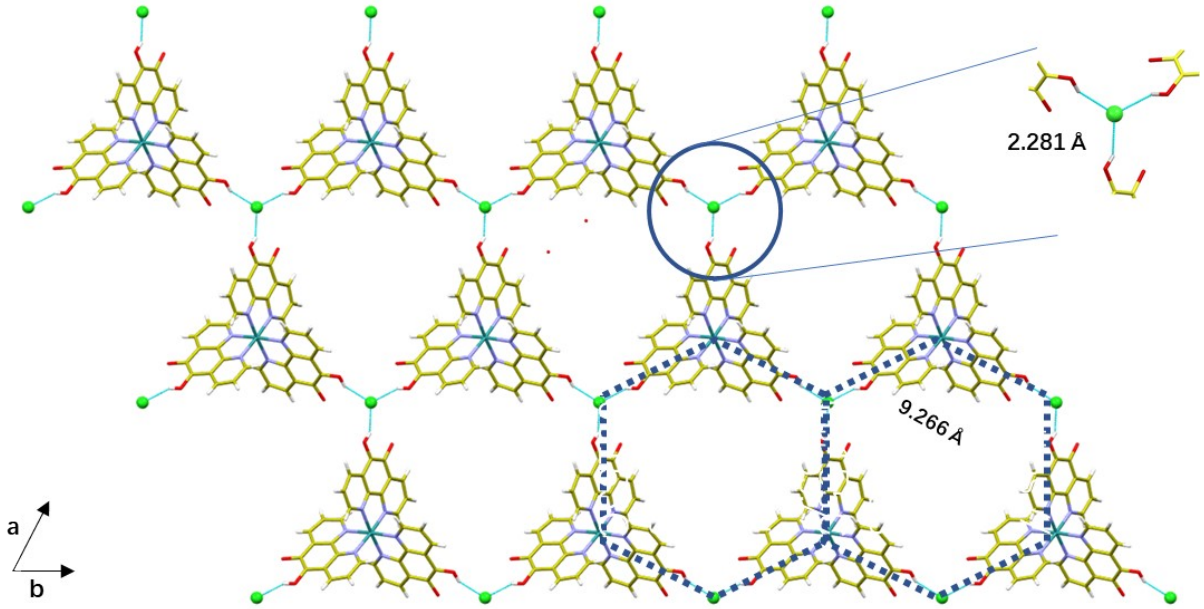

Figure S6: H-bond network in one layer of **1.Cl** consisting of [Ru(5,6-dihydroxy-1,10-phenanthroline)$_2$(5-oxido-6-hydroxy-1,10-phenanthroline)]$^+$ cations and chloride anions (green sphere) highlighting hexagonal pores.

In the crystal lattice of **1.Cl**, each Cl^- ion is hydrogen bonded with one catechol hydroxyl group of three neighboring Ru-phenanthroline subunits (O···Cl: 3.043Å, O–H···Cl: 2.281Å, ∠ClHO: 150.69°) in a trifurcated manner which extends in the *ab* plane. This H-bonded triad represents a nearly perfect tetrahedron where the Cl^- ions lie *ca*. 0.63 Å above the basal plane formed by three hydroxyl oxygens (∠OClO ~109.6°; O···O ~4.974Å). The average O–H···Cl hydrogen bond distance is *ca*. 76% *vdW* which is in accordance with the previously reported catechol-chloride H-bonded organic frameworks. This supramolecular association extends in the *ab*-plane to form honeycomb (***hcb***) network with hexagonal pores consisting of Ru(II) cations and anions as corners, and aromatic phenanthroline ligands as edges (Figure 2). The large perfect hexagonal pores have edge length of *ca.* 9.266 Å (Ru···Cl distance) leading to large pore window of ~223 Å^2 where the phenanthroline rings are out of the plane connecting Ru and Cl ions by *ca*. 30°.

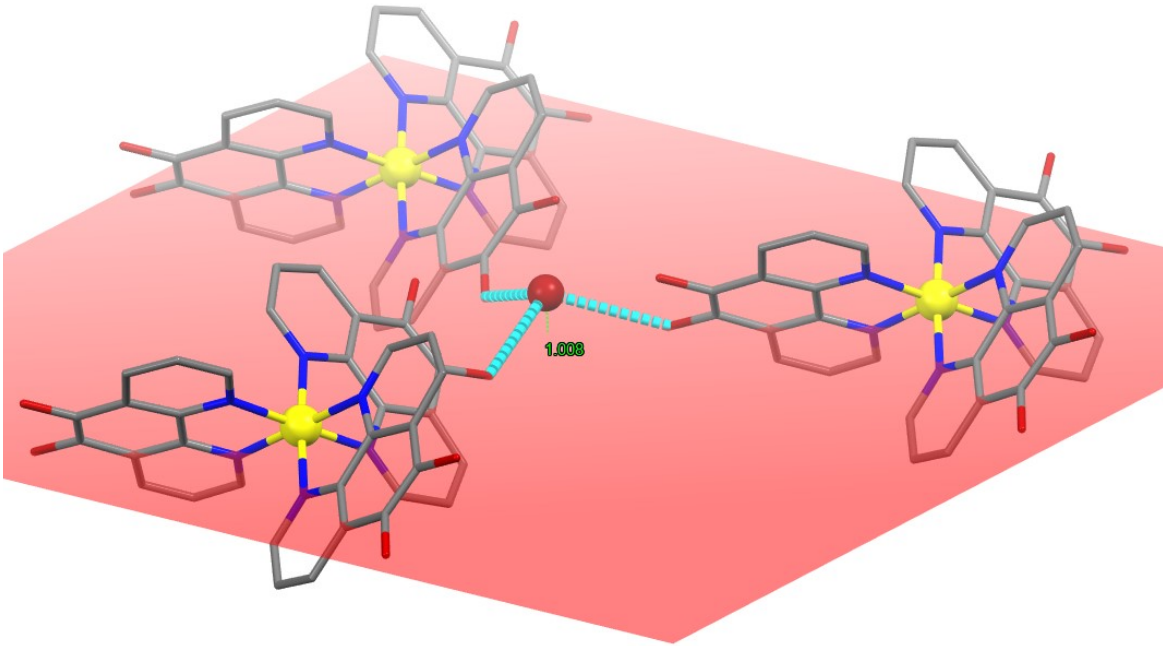

Figure S7: One Cl^- anion holding three coordination complex units at nearly 1.008 Å above the basal plane formed by three H-bonded oxygen atoms.

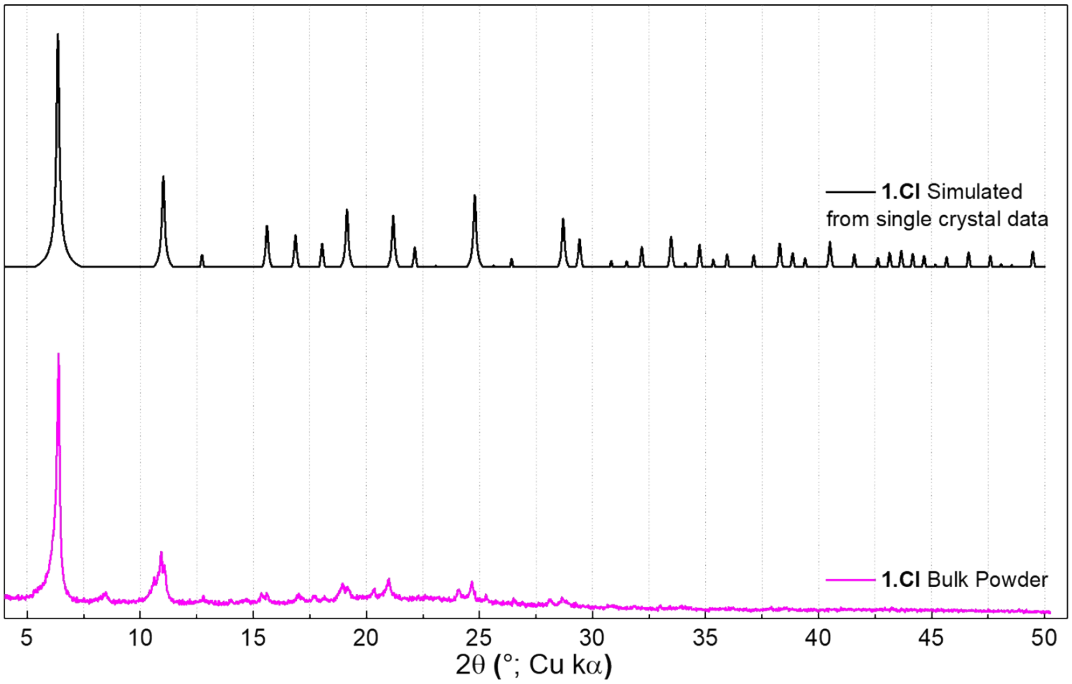

Figure S8: Comparison of powder XRD patterns of bulk powder of **1.Cl** with the corresponding simulated diffractogram from single-crystal data.

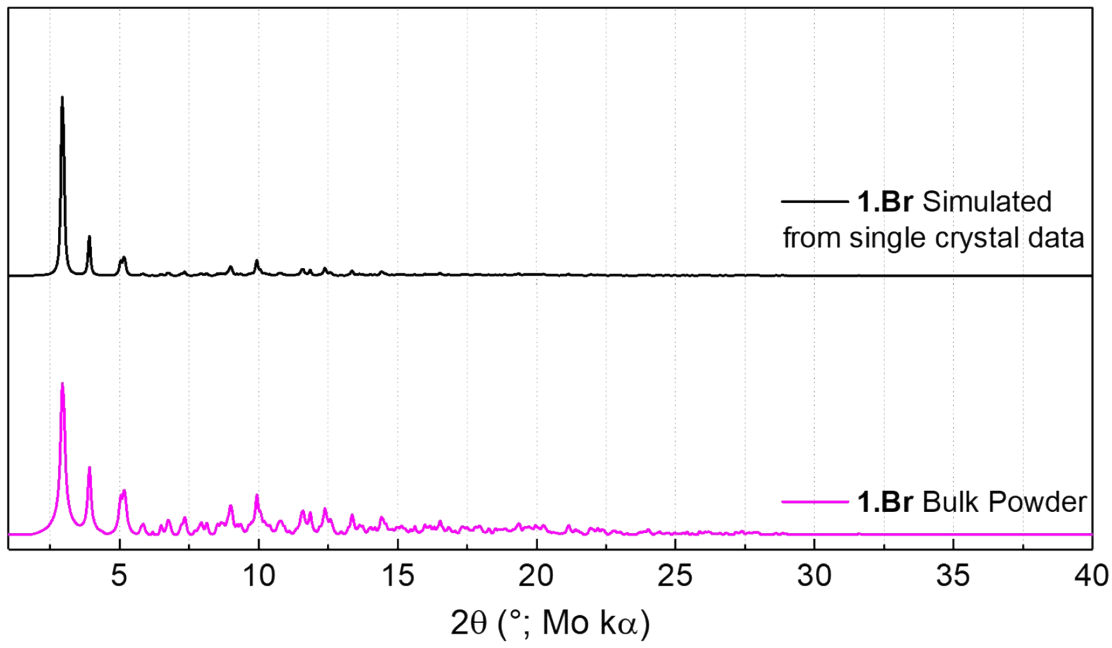

Figure S9: Comparison of XRD patterns of bulk powder of **1.Br** with the corresponding simulated diffractogram from single-crystal data.

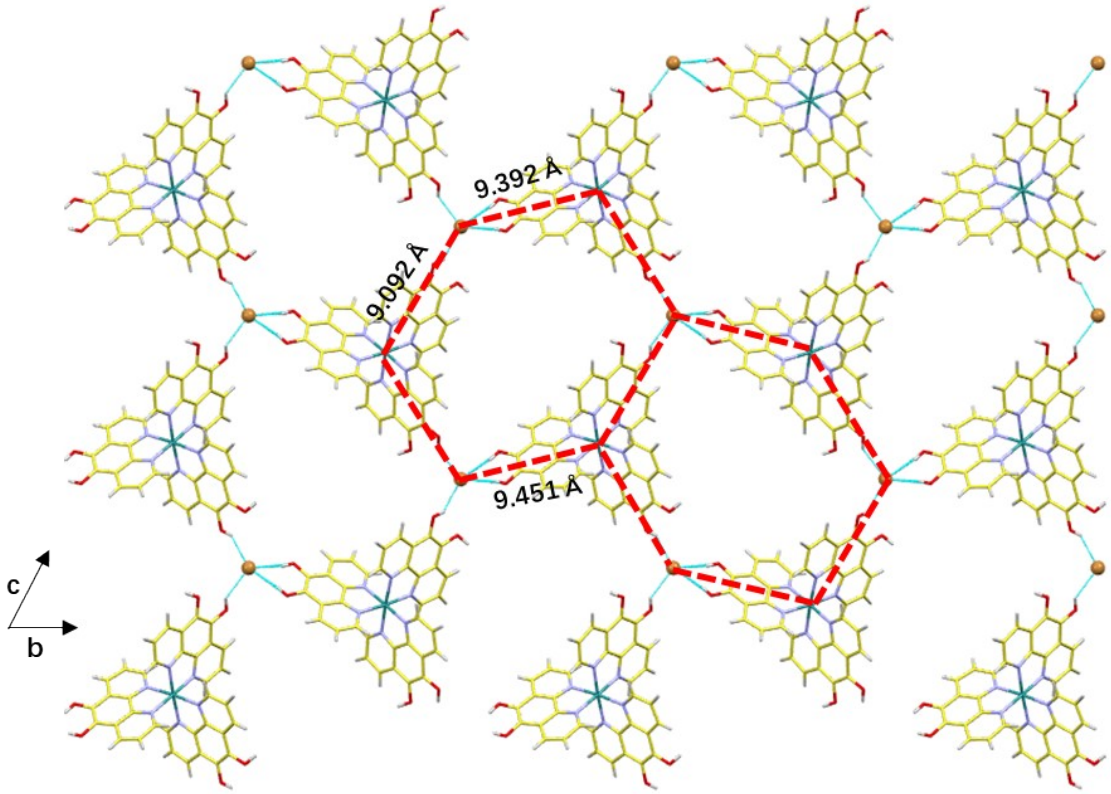

Figure S10: H-bond network in one layer of **1.Br** consisting of [Ru(5,6-dihydroxy-1,10-phenanthroline)$_2$(5-oxido-6-hydroxy-1,10-phenanthroline)]$^+$ cations and bromide anions (brown spheres) highlighting distorted hexagonal pores.

Br^- ions displayed similar anion-template effect in **1.Br** *via* weaker O−H···anion interactions with four nearby hydroxyl groups from three building block units (*avg.* O···Br ~3.127 Å, *avg*. O−H···Br ~2.373 Å, *avg*. ∠BrHO ~154.46°) (Figure 2). In the H-bonded quadruple, one of the building blocks forms convergent hydrogen bonds to the Br^- ion through both of the hydroxyl groups. Unlike **1.Cl**, the pores are not perfectly hexagonal and rather skewed which is presumably due to higher ionic radii of Br^- ions.

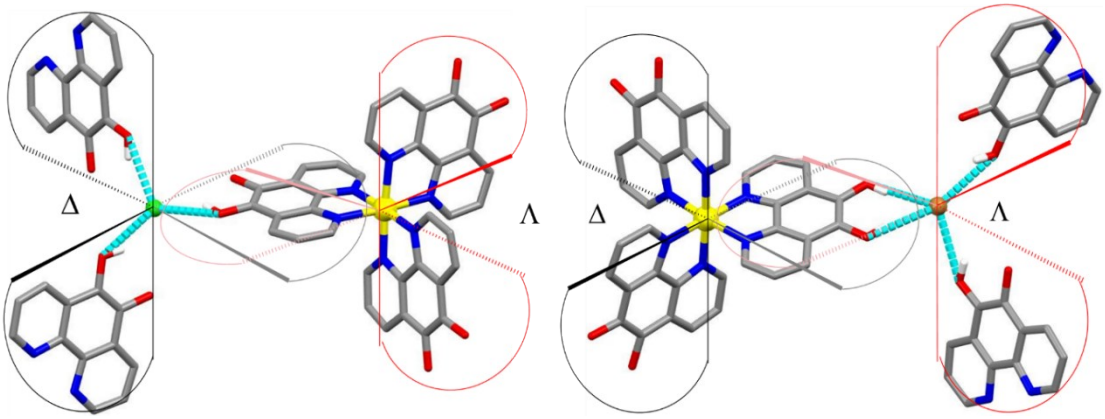

Figure S11: Stereochemistry around the Ru(II) cation in the complex and anions in **1.Cl** (left) and **1.Br** (right).

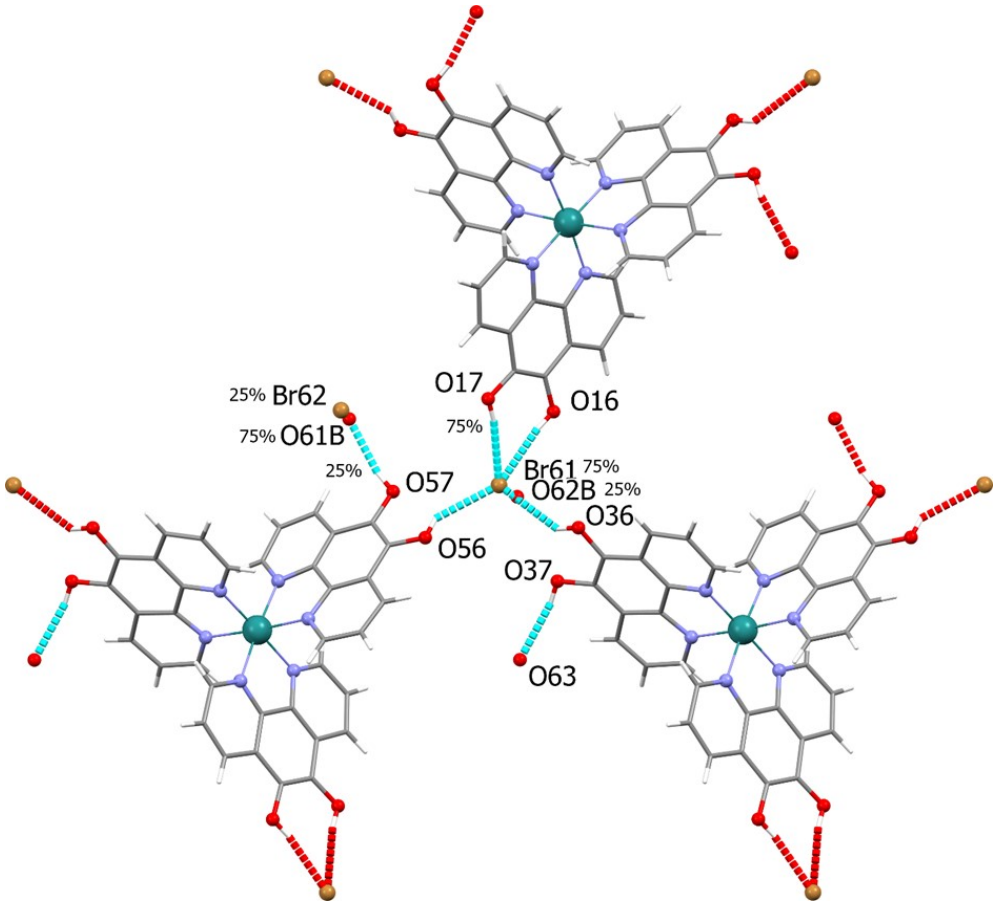

Figure S12: Hydrogen bond interactions involving the Br (Br61/Br62) anions and water molecules (O61B/O62B and O63), the occupancies are indicated.

In **1.Br**, a similar cation-complex/anion ratio was found, although the Bromide anion was found to be disordered over two separate sites existing roughly in the ratio of 75/25, the vacant space is occupied by a disordered water molecule in the revresed ratio (25/75). The major Bromide site interacts with three phenanthroline ligands from neighboring complex. i.e. either the bromide or water molecule is involved in a hydrogen bond with one of the OH groups (O16, O36, O56). The OH (O37) is engaged in a full H-bond with the fully occupied lattice water molecule O63. This means the negative charge is distributed over O17 and O57. The hydrogen atoms on those oxygen atoms also hydrogen bond to the bromide atoms. This results in a 75% occupancy for H17 interacting with Bromide Br61 (at 75% occupancy) and a 25% occupancy for H57 interacting with Br62 (at 25% occupancy); leaving a net negative charge of –3/4 on O57 and –1/4 on O17.

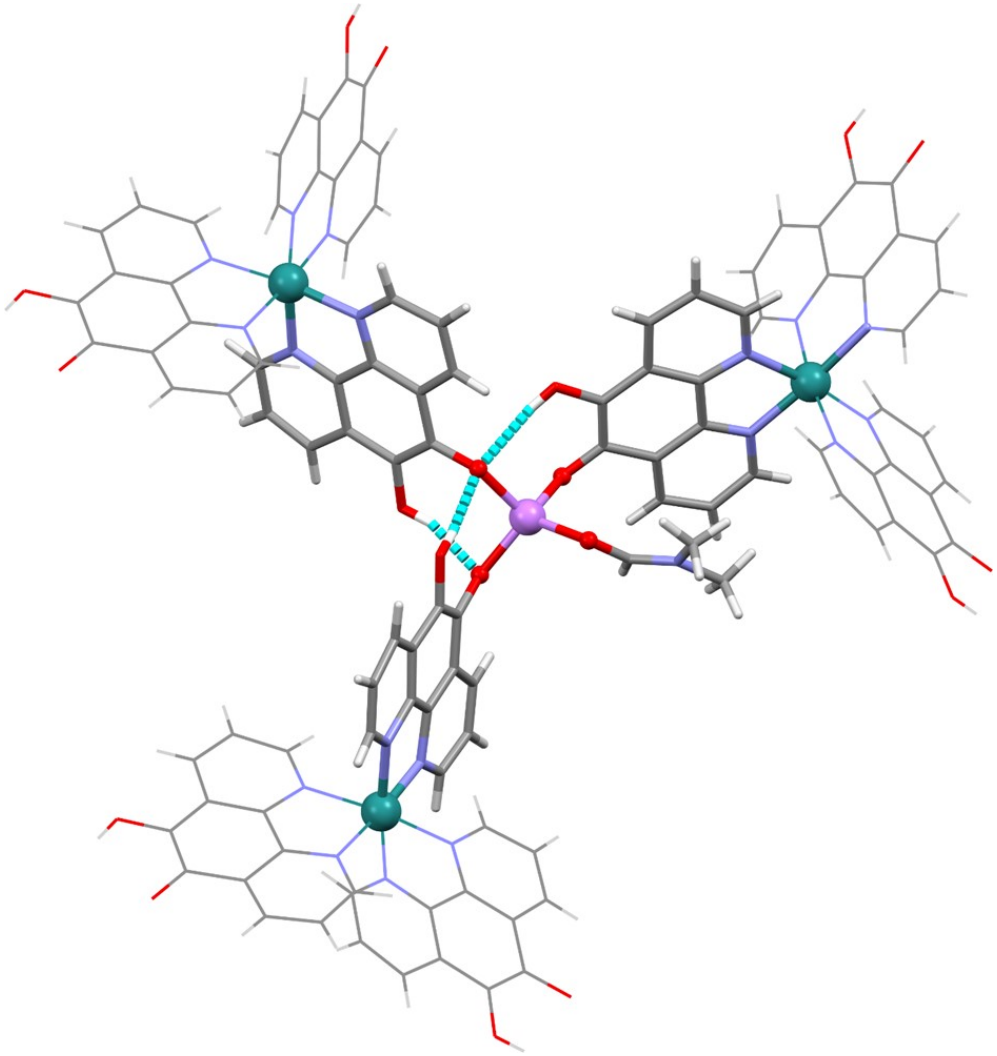

Figure S13: Tetragonal geometry around Li (purple) in **1.Li** involving three C-O groups and one DMF molecule. The OH groups are hydrogen bonded to neighboring C-O groups.

For **1.Li** the charge distribution is more straightforward, the total positive charge comprises of 1 Ru(II) and 1 Li(I) and is compensated by a negative charge on every phenanthroline ligand. Every Li cation is in a tetragonal configuration with 3 phenanthroline ligands, through the C-O^-, and 1 oxygen atom of a DMF solvent molecule. The OH groups hydrogen bond to neighboring C-O^- oxygen atoms.

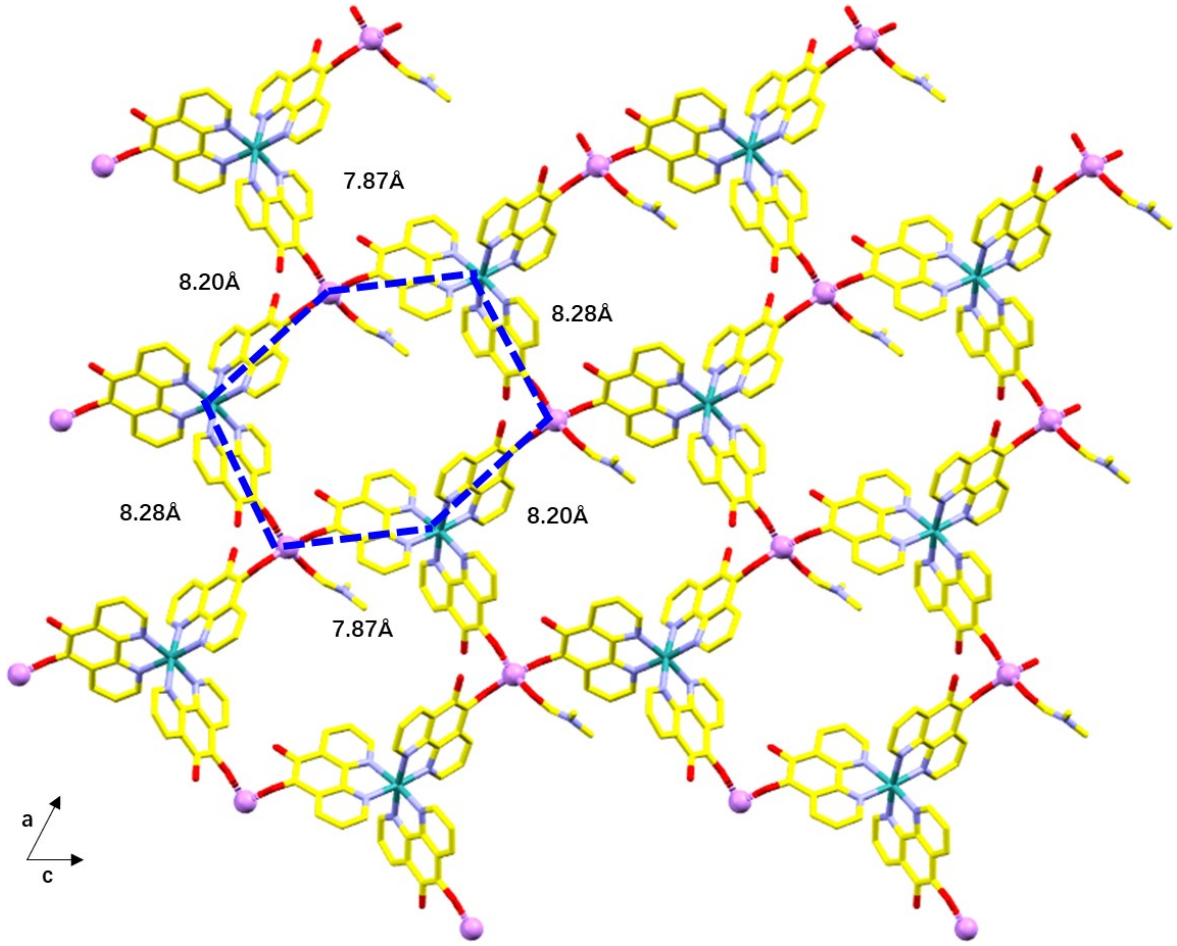

Figure S14: H-bond network in one layer of **1.Li** consisting of [Ru(5-oxido-6-hydroxy-1,10-phenanthroline)$_3$] anion and Li^+ cations (pink spheres) highlighting distorted hexagonal pores.

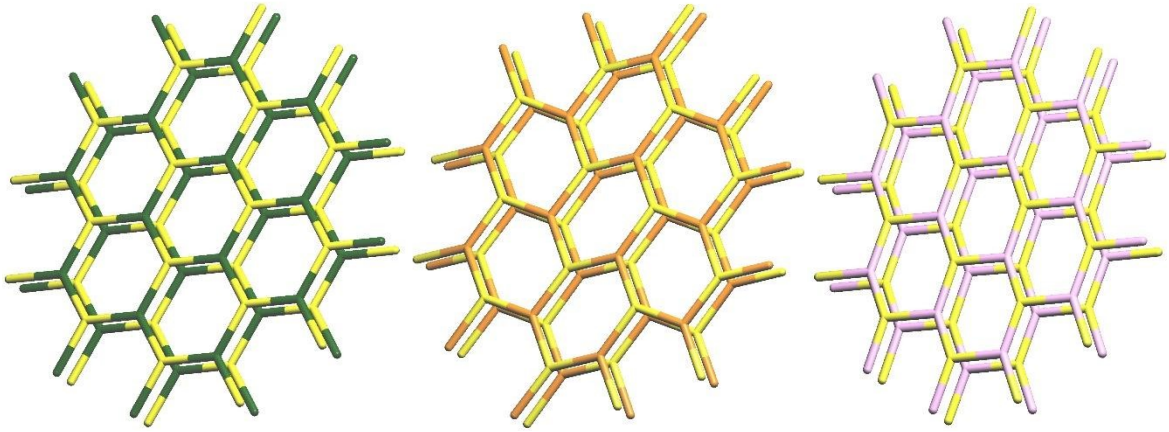

Figure S15: A topological stack of two 2D layers showing hexagonal (6^3) net of **1.Cl** (left), **1.Br** (center) and **1.Li** (right).

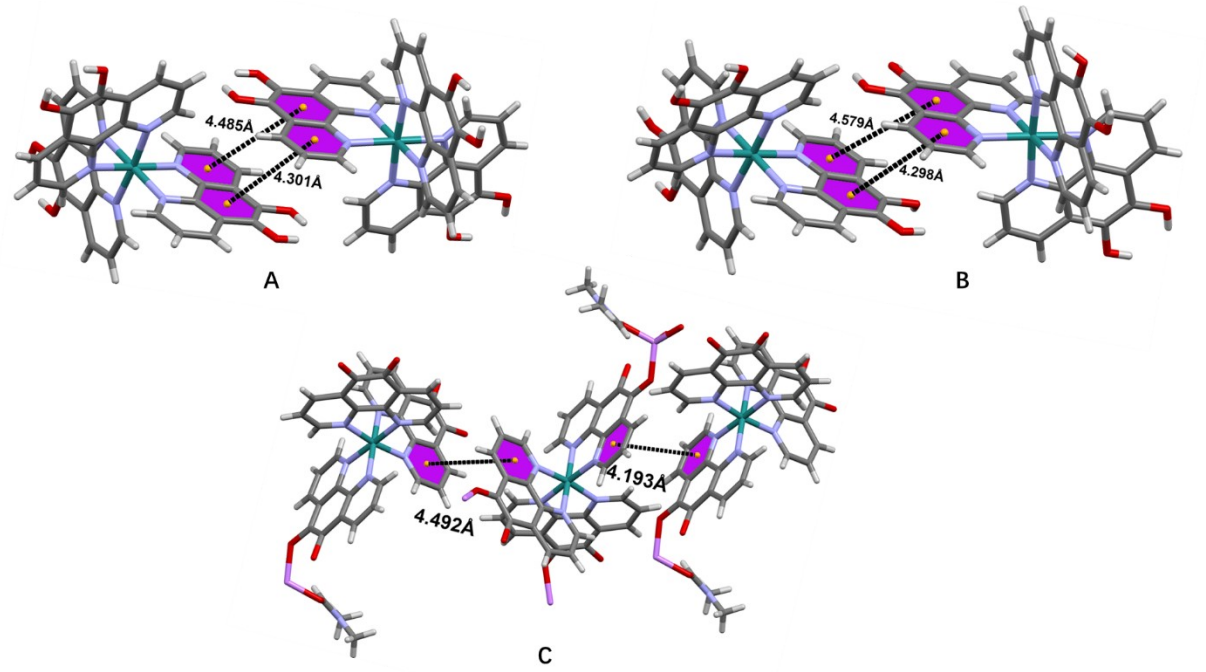

Figure S16: Aromatic stacking interactions between adjacent molecules of **1.Cl** (A), **1.Br** (B) and **1.Li** (C).

Thermal stability of 1.Cl and 1.Br

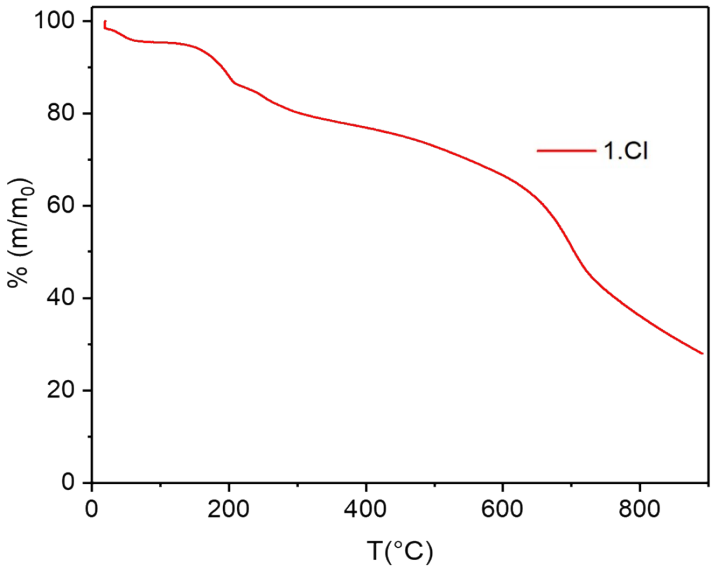

Figure S17: Thermogravimetric (TGA) profile showing the decomposition of **1.Cl** in the temperature range from 20°C to 900°C.

A 4.55% loss at an average temperature of 40°C is observed and 9.75% of loss appears at a 150°C temperature average. The loss refers to a complete removal of residual ethanol and diethylether (residual low boiling solvents stuck in the network), as well as H_2O molecules*. A clear plateau between the first two losses suggests that two well distinct solvent removal or other processes appear successively one after another. A 7.86% of mass weight was lost at an average of 250°C temperature. After 300°C, the decomposition of the complex gradually occurs until the end of the analysis at 900°C.

** Important to note, the conditions of measurements of such an analysis requires a very short exposure to air to transfer the sample in the machine. This inevitably provokes the adsorption of few H_2O molecules, also responsible for the early weight loss below 100°C.*

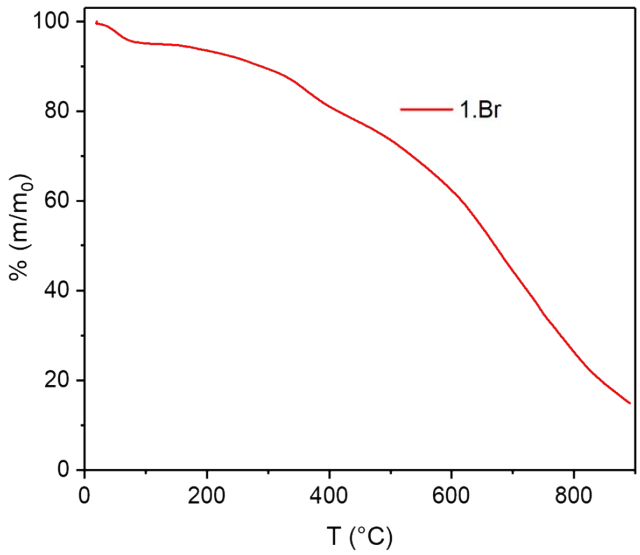

Figure S18: Thermogravimetric (TGA) profile showing the decomposition of **1.Br** in the temperature range from 20°C to 900°C.

A loss of 5.07% at 60°C was observed, corresponding to a complete removal of residual ethanol and diethylether molecules (and H_2O molecules given that sample are inevitably exposed to ambient air before loading in the TGA machine). A plateau is then observed until 175°C which is showing the thermal stability of the complex. After, the decomposition of the complex occurs from 200°C to 900°C with a rather constant slope.

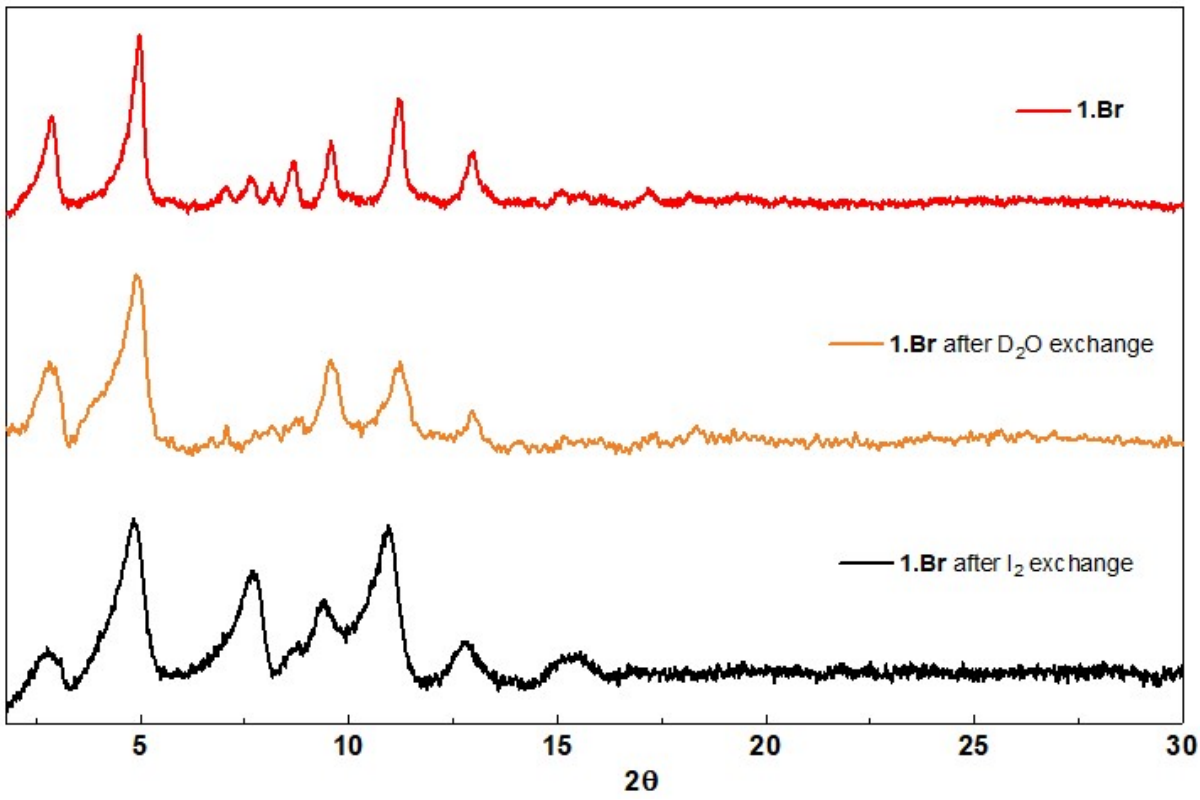

Figure S19: Comparative PXRD patterns of **1.Br** (red), after D_2O exchange (orange) and after iodine exchange (black).

SI-References:

1. Wendlandt, A. E., Stahl, S. S., *J. Am. Chem. Soc.*, **2014**, 136, 34, 11910-11913.

2. Paw, W., and Eisenberg, R., Synthesis, Characterization and Spectroscopy of Dipyridocatecholate Complexes of Platinum, *Inorg. Chem*., 1997, **36**, 2287-2293.

3. Lakraychi, A. E., *et al.*, Phendione–Transition-Metal Complexes with Bipolar Redox Activity for Lithium Batteries, *ChemSusChem*, 2020,**13**, 9, 2225-2231.

4. Halis, S., Inge, A. K., Dehning, N., Weyrich, T., Reinsch, H., & Stock, N., Dihydroxybenzoquinone as Linker for the Synthesis of Permanently Porous Aluminum Metal–Organic Frameworks, *Inorganic Chemistry*, 2016**, 55**, 15, 7425-7431

5. Raj, J. G. J., Pathak, D. D., & Kapoor, P. N. (2013). Multi-Nuclear NMR Investigation of Nickel (II), Palladium (II), Platinum (II) and Ruthenium (II) Complexes of an Asymmetrical Ditertiary Phosphine. *Journal of the Korean Chemical Society*, 2013, **57**, 6, 726-730.

6. CrysAlisPro, version 1.171.33.49b, Oxford Diffraction Ltd., Abingdon, UK, **2009**.

7. Sheldrick, G. M., SHELXT - Integrated space-group and crystal-structure determination. *Acta Crystallographica Section A: Foundations of Crystallography*, 2015, **71**, 3–8.

8. Sheldrick, G. M., Crystal structure refinement with SHELXL. *Acta Crystallographica Section C: Structural Chemistry*, 2015, **71**, 3–8.

9. Spek, A. L. Structure validation in chemical crystallography. *Acta Crystallogr.* 2009, **D65**, 148–155.